

Yik R. Teo

Precision Mechatronics Lab,
School of Electrical Engineering and
Computer Science,
The University of Newcastle,
Callaghan, New South Wales 2308, Australia
e-mail: yik.teo@newcastle.edu.au

Andrew J. Fleming

Precision Mechatronics Lab,
School of Electrical Engineering and
Computer Science,
The University of Newcastle,
Callaghan, New South Wales 2308, Australia
e-mail: andrew.fleming@newcastle.edu.au

Arnfinn A. Eielsen

Department of Engineering Cybernetics,
Norwegian University of Science and Technology,
Trondheim NO-7491, Norway
e-mail: eielsen@itk.ntnu.no

J. Tommy Gravdahl

Department of Engineering Cybernetics,
Norwegian University of Science and Technology,
Trondheim NO-7491, Norway
e-mail: gravdahl@itk.ntnu.no

A Simplified Method for Discrete-Time Repetitive Control Using Model-Less Finite Impulse Response Filter Inversion

Repetitive control (RC) achieves tracking and rejection of periodic exogenous signals by incorporating a model of a periodic signal in the feedback path. To improve the performance, an inverse plant response filter (IPRF) is used. To improve robustness, the periodic signal model is bandwidth-limited. This limitation is largely dependent on the accuracy of the IPRF. A new method is presented for synthesizing the IPRF for discrete-time RC. The method produces filters in a simpler and more consistent manner than existing best-practice methods available in the literature, as the only variable involved is the selection of a windowing function. It is also more efficient in terms of memory and computational complexity than existing methods. Experimental results for a nanopositioning stage show that the proposed method yields the same or better tracking performance compared to existing methods. [DOI: 10.1115/1.4033274]

1 Introduction

Repetitive control is a well-known control technique used in systems to track and reject periodic exogenous signals [1]. This is achieved due to the internal model principle [2], which states that an exogenous signal (e.g., a reference or disturbance) can be nulled in the error signal if a model of the dynamic structure of the exogenous signal is in the feedback path. RC was originally developed to reject the periodic disturbances in a power supply control application [3,4], but has since been used for machining of parts [5], precision positioning [6], optical drives [7–9], electrohydraulics [10], and scanning probe microscopy [11–13].

Figure 1 shows the ideal signal model used in RC for a periodic signal with period L . This is a computationally efficient and numerically stable implementation, as the model only consists of a positive feedback around a time delay. This results in an infinite number of marginally stable poles with infinite gain at the harmonics of the periodic reference.

The most common implementation of discrete-time RC was first proposed in Ref. [14]. Here, the plant dynamics is inverted using the zero-phase error tracking control (ZPETC) method. By doing so, a signal model bandwidth up to the Nyquist frequency can in principle be obtained. However, the approach lacks robustness, especially in plant modeling errors. The most common solution to this problem is to limit the signal model bandwidth using a low-pass filter [1,15,16]. This improves the stability margin at higher frequencies, where the plant model typically has the largest uncertainty. An alternative to this approach is the application of general uncertainty and performance weights, which can be accommodated for using the \mathcal{H}_∞ synthesis framework [17,18], or the robustness can be improved by computing a frequency weighted inverse of the plant [19].

In order to achieve high signal model bandwidth, the ZPETC inverse requires an accurately identified infinite impulse response (IIR) model of the plant. The accuracy of the identified model depends on the choice of model structure, the excitation signal, and the estimation method. In addition, since nonminimum phase zeros cannot be inverted, the magnitude response of the ZPETC inverse can be inaccurate. Nonminimum phase zeros are typically introduced due to sampling. Thus, inversion effectiveness depends on model accuracy and the effect of the nonminimum phase zeros. The best IIR model estimation methods currently available are arguably subspace methods [20,21]. Subspace methods require high accuracy numerical linear algebra, and can be computationally demanding. Furthermore, the ZPETC method requires the solution of an eigenvalue problem, and numerical linear algebra is again needed.

As an alternative to the IIR model inverse, a finite impulse response (FIR) filter inverse model can be used [22,23]. An FIR filter can alleviate problems due to nonminimum phase zeros and the selection of model structure. The main disadvantage is that an FIR filter can be more computationally demanding than an IIR filter. The synthesis of an inverse plant response FIR filter based on minimizing a least-squares cost function in the frequency domain was proposed in Refs. [22,23]. This is equivalent to the least-squares method for FIR filter synthesis [24]. However, the two most salient problems with this approach is that there are no

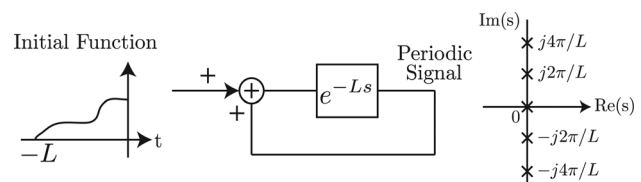


Fig. 1 A time delay with positive feedback with the appropriate initial function can model any periodic signal [1]

Contributed by the Dynamic Systems Division of ASME for publication in the JOURNAL OF DYNAMIC SYSTEMS, MEASUREMENT, AND CONTROL. Manuscript received July 26, 2015; final manuscript received March 23, 2016; published online May 24, 2016. Assoc. Editor: Ming Xin.

guidelines on the choice of FIR filter length, and that an ad-hoc error weighting function has to be chosen for the cost function in order to synthesize a filter with an accurate enough fit to ensure closed-loop stability. Additionally, the least-squares problem can be computationally demanding for long FIR filters and requires linear algebra with sufficient numerical accuracy.

In either case, for both the IIR and the FIR filter, one of the most reliable methods of identification is to fit filter coefficients by way of an empirical transfer function estimate (ETF) [21]. In Refs. [19,22], and [23], it is suggested to generate an ETF using Welch's averaged periodogram method [25]. In order to obtain an accurate ETF using this method, a suitable excitation signal has to be chosen and a large dataset has to be collected. This is needed to reduce the effect of noise. Furthermore, choices have to be made in regard to windowing, section overlapping, and number of frequency lines—all of which will influence the quality of the estimate. Finding good power spectral density estimates with Welch's method can therefore be tedious, and the method is computationally demanding.

In this paper, alternative methods for producing the ETF as well as an inverse plant response FIR filter are presented. Here, the ETF is computed directly using the discrete Fourier transform (DFT), using a time series generated by way of pseudorandom binary signal (PRBS) excitation and subsequent periodic averaging in the time domain. By using periodic averaging, high accuracy is ensured. The inverse plant response FIR filter is then computed directly using the inverse DFT (IDFT) of the inverse of the ETF, and a suitable windowing function. This last step is equivalent to the frequency sampling method for FIR filter synthesis [26]. Producing the ETF in this manner reduces the computational and memory requirements, and it dispenses of the need to use any numerical linear algebra, as only the DFT and IDFT are needed. It also avoids the tuning in terms of windowing, section overlapping, and number of frequency lines. Furthermore, the filter synthesis can be done without any of the modeling effort needed for the ZPETC inverse, and without the effort to find a suitable filter length and error weighting function needed for the optimization-based FIR filter inverse in Refs. [22,23]. The frequency sampling method for FIR filter synthesis only requires a choice of windowing function; thus, the presented approach produces more consistent results and simplifies the design process. Experimental results are provided to show that the proposed approach produces the same, or better, results than when using the ZPETC or the optimization-based FIR filter inverse.

2 Discrete-Time RC

Figure 2 shows a block diagram for a general RC scheme applied to a plant $G(z^{-1})$. The filters $H_1(z^{-1})$ and $H_2(z^{-1})$ are used to produce a bandwidth-limited signal generator. If $H_1(z^{-1})$ and $H_2(z^{-1})$ have linear-phase, and therefore constant group delay, then a group delay of L will produce poles at $\pm j2\pi n/L$, $n \in \mathbb{N}_0$. Symmetric FIR filters have a linear-phase response which is why, ideally, $H_1(z^{-1})$ and $H_2(z^{-1})$ are chosen to be such filters. The magnitude response of $H_1(z^{-1})$ and $H_2(z^{-1})$ can then be used to limit the bandwidth. $H_3(z^{-1})$ is the IPRF, implemented as either an IIR or FIR filter.

From Fig. 2, it can be seen that the RC scheme is equivalent to the control law

$$C(z^{-1}) = \frac{H_1(z^{-1})H_3(z^{-1})}{1 - H_1(z^{-1})H_2(z^{-1})} \quad (1)$$

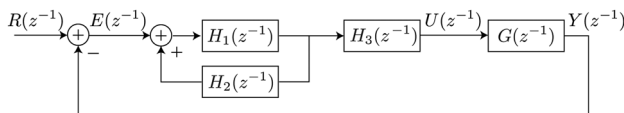


Fig. 2 Block diagram for a general RC system

Assuming that the reference signal period will always be an integer multiple of the sampling time T_s , the product of $H_1(z^{-1})H_2(z^{-1})$ in the denominator has to contain a delay of z^{-N} , where

$$N = \frac{L}{T_s} \quad (2)$$

to satisfy the internal model principle.

The sensitivity function, the transfer-function from the reference $R(z^{-1})$ to the error $E(z^{-1})$ in closed-loop, is

$$S(z^{-1}) = \frac{1 - H_1(z^{-1})H_2(z^{-1})}{1 - H_1(z^{-1})(H_2(z^{-1}) - H_3(z^{-1})G(z^{-1}))} \quad (3)$$

which can be rearranged to be on the form shown in Fig. 3. It can then be seen that the stability of the RC system is determined by the denominator

$$1 - H_1(z^{-1})(H_2(z^{-1}) - H_3(z^{-1})G(z^{-1}))$$

which will provide stability if the loop transfer function in Fig. 3 satisfies the small-gain theorem [14,19]. Thus, the system is stable if

$$\|H_1(z^{-1})(H_2(z^{-1}) - H_3(z^{-1})G(z^{-1}))\|_\infty < 1 \quad (4)$$

The stability condition can be split into two conditions, i.e.,

$$\|H_1(z^{-1})\|_\infty < 1 \quad (5)$$

and

$$\|H_2(z^{-1}) - H_3(z^{-1})G(z^{-1})\|_\infty < 1 \quad (6)$$

These two stability conditions are necessary for the design of RC as it is done in this paper.

3 Synthesizing IPRFs

The IPRFs can be made using either a model-based IIR filter or a model-less FIR filter. The model-based IIR filter discussed here is synthesized using the ZPETC [27]. The synthesis of the model-less FIR filter is first shown using frequency domain optimization [22,23], equivalent to the least-squares method for FIR filter synthesis [24], and is then followed by a presentation of the method proposed in this article; equivalent to the frequency sampling method for FIR filter synthesis [26].

3.1 Model-Based IIR Filter Synthesis. An IIR filter model of the plant is given as

$$\hat{G}_{\text{IIR}}(z^{-1}) = z^{-d} \frac{B(z^{-1})}{A(z^{-1})} \quad (7)$$

where z^{-d} is the dead time of the plant, and

$$B(z^{-1}) = b_0 + b_1 z^{-1} + \dots + b_{m_b} z^{-m_b}, \quad b_0 \neq 0$$

$$A(z^{-1}) = 1 + a_1 z^{-1} + \dots + a_{n_a} z^{-n_a}$$

More details on how to identify the coefficients of the IIR filter are discussed in Sec. 4.

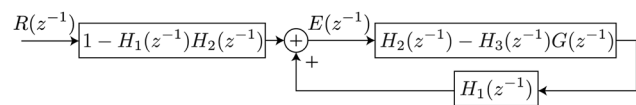


Fig. 3 Equivalent description of sensitivity function

The perfect feedforward tracking control law for Eq. (7) is

$$\widehat{G}_{\text{IIR}}^{-1}(z^{-1}) = z^d \frac{A(z^{-1})}{B(z^{-1})}$$

which is noncausal due to the inverse of the d -step delay. The inverse cancels all the poles and zeros such that the product of the inverse filter and the plant is unity, i.e., there is zero-phase shift. This is only possible if the roots of $B(z^{-1}) = 0$ are inside the unit circle in the z -plane, which means they are minimum phase zeros.

The method of inversion that excludes the nonminimum phase zeros is called the ZPETC [27]. Applying this inverse, the product of the inverse filter and the plant will have zero-phase shift. This is done by factorizing the zeros of $\widehat{G}(z^{-1})$ as

$$B(z^{-1}) = B_a(z^{-1})B_u(z^{-1})$$

where $B_a(z^{-1})$ includes minimum phase (acceptable) zeros, and $B_u(z^{-1})$ includes nonminimum phase (unacceptable) zeros. The ZPETC inverse is then found to be [27]

$$F_{\text{ZPETC}}(z^{-1}) = z^{(d+m_s)} \frac{A(z^{-1})\bar{B}_u(z^{-1})}{B_a(z^{-1})[B_u(1)]^2}$$

where $B_u(1)$ is the direct current (DC) gain of $B_u(z^{-1})$, and

$$\bar{B}_u(z^{-1}) = \bar{b}_{m_s} + \bar{b}_{(m_s-1)}z^{-1} + \dots + \bar{b}_0z^{-m_s}$$

The filter is noncausal and $d + m_s$ steps ahead. This can be overcome by delaying the input. As a result, the filter $H_3(z^{-1})$ is taken to be

$$H_3(z^{-1}) = z^{-(d+m_s)}F_{\text{ZPETC}}(z^{-1})$$

RC requires that the product of the filters $H_1(z^{-1})$ and $H_2(z^{-1})$ has a delay of N steps. The stability criterion (6) is most easily satisfied if

$$H_2(z^{-1}) = z^{-(d+m_s)}$$

since $|H_2(z^{-1})| = |e^{-j\omega(d+m_s)}| = 1$, and thus Eq. (6) is

$$\begin{aligned} & \|z^{-(d+m_s)} - z^{-(d+m_s)}F_{\text{ZPETC}}(z^{-1})G(z^{-1})\|_{\infty} \\ &= \|1 - F_{\text{ZPETC}}(z^{-1})G(z^{-1})\|_{\infty} < 1 \end{aligned}$$

where $F_{\text{ZPETC}}(z^{-1})G(z^{-1}) \approx 1$ if the ZPETC inverse is accurate. Assuming $N > d + m_s$, $H_1(z^{-1})$ can be chosen to be a linear-phase FIR filter with a delay of $N - d - m_s$, i.e., it will have an order of $2(N - d - m_s)$, which means that it will have $2(N - d - m_s) + 1$ taps. $H_1(z^{-1})$ is a low-pass filter used to satisfy Eq. (4) at higher frequencies, where the uncertainty of the ZPETC inverse typically is high. In the presence of more severe uncertainty, the method for synthesizing a frequency-weighted IIR filter inverse of the plant in Ref. [19] might be a better option.

3.2 Model-Less FIR Filter Synthesis. The alternative to the model-based IIR filter is to use an FIR filter. This can be considered a model-less approach because no model structure needs to be chosen. An FIR filter alleviates problems due to nonminimum phase zeros and the selection of model structure present when using an IIR filter.

3.2.1 Optimization-Based FIR Filter Synthesis. Synthesizing an FIR filter which approximates the inverse of the system based on frequency domain optimization for use in RC was initially shown in the implementation suggested in Refs. [22,23]. The method is equivalent to the least-squares method for FIR filter synthesis [24].

Here it is assumed that an ETFE of the plant is available. In terms of frequency samples $k \in [0, M - 1] \cap \mathbb{N}_0$, the ETFE of the plant is denoted $\widehat{G}(k)$, and its inverse is denoted $\widehat{G}^{-1}(k)$. How to obtain an ETFE is discussed in Sec. 4.

An FIR filter transfer function is given as

$$F_1(z^{-1}) = z^q(a_0 + a_1z^{-1} + \dots + a_{p-1}z^{-p+1}) = z^q \mathbf{a}^T \mathbf{z} \quad (8)$$

where $p, q \in \mathbb{N}_0$

$$\mathbf{a} = [a_0, a_1, \dots, a_{p-1}]^T, \text{ and } \mathbf{z} = [1, z^{-1}, \dots, z^{-p+1}]^T$$

A desired filter length p must be chosen, and q is given as

$$q = \begin{cases} p/2, & \text{if } p \text{ is even} \\ (p+1)/2, & \text{if } p \text{ is odd} \end{cases} \quad (9)$$

The filter length p is chosen based on trial and error [22].

The coefficient \mathbf{a} in Eq. (8) is found by minimizing the weighted least-squares cost of the error

$$\epsilon(k) = F_1(e^{-j2\pi k/M}) - \widehat{G}^{-1}(k) = \mathbf{a}^T \mathbf{x}_k - \widehat{G}^{-1}(k) \quad (10)$$

using $z = e^{j2\pi k/M}$ and where

$$\mathbf{x}_k = \left[e^{-j\frac{2\pi k(-q)}{M}}, e^{-j\frac{2\pi k(1-q)}{M}}, \dots, e^{-j\frac{2\pi k(p-q)}{M}} \right]^T$$

that is, minimizing the standard weighted linear least-squares cost function [24,28]

$$J(\mathbf{a}) = \sum_{k=0}^{M-1} V(k)\epsilon(k)\epsilon^*(k) = \|\mathbf{V}^{1/2}(\mathbf{b} - \mathbf{X}\mathbf{a})\|^2 \quad (11)$$

where $V(k)$ is an error weighting function [24,28]

$$\begin{aligned} \mathbf{V} &= \text{diag}([V(0), V(1), \dots, V(M-1)]^T), \\ \mathbf{b} &= \begin{bmatrix} \widehat{G}^{-1}(0) \\ \widehat{G}^{-1}(1) \\ \vdots \\ \widehat{G}^{-1}(M-1) \end{bmatrix}, \text{ and } \mathbf{X} = \begin{bmatrix} \mathbf{x}_0^T \\ \mathbf{x}_1^T \\ \vdots \\ \mathbf{x}_{M-1}^T \end{bmatrix} \end{aligned}$$

where $\mathbf{V} \in \mathbb{R}^{M \times M}$, $\mathbf{b} \in \mathbb{R}^{M \times 1}$, $\mathbf{X} \in \mathbb{R}^{M \times M}$. The error weighting function can be used to adjust how to weigh the error at different frequencies. Choosing a reasonable weighting function can be difficult, but a good guideline is to weigh the data inversely to the uncertainty of it [28]. For example, for most ETFEs, the uncertainty is high at high frequencies; a low weight should therefore be chosen for the high frequency data. The MATLAB function `lscov` can be used to minimize Eq. (11).

Alternatively, in Ref. [22], the cost function

$$J_2(\mathbf{a}) = \|1 - \text{diag}(\mathbf{b})^{-1} \mathbf{X}\mathbf{a}\|^2$$

is proposed. This is equivalent to using the weight

$$\mathbf{V}^{1/2} = \text{diag}(\mathbf{b})^{-1}, \quad \text{or} \quad V(k) = |\widehat{G}(k)|^2 \quad (12)$$

in Eq. (11), i.e., weighing by the magnitude of the ETFE. This weighing is entirely dependent on a particular ETFE, that is, a measured response. It can therefore give unexpected results if noise or nonideal effects has corrupted the data. It cannot be expected that this weighing will yield good results in general.

The filter $F_1(z^{-1})$ is noncausal and q steps ahead; thus, to obtain causality in the implementation, the input must be delayed. As a result, the filter $H_3(z^{-1})$ is taken to be

$$H_3(z^{-1}) = z^{-q}F_1(z^{-1})$$

RC requires that the product of the filters $H_1(z^{-1})$ and $H_2(z^{-1})$ has a delay of N steps. The stability criterion (6) is most easily satisfied if

$$H_2(z^{-1}) = z^{-q}$$

since $|H_2(z^{-1})| = 1$, and thus Eq. (6) is

$$\|z^{-q} - z^{-q}F_1(z^{-1})G(z^{-1})\|_\infty = \|1 - F_1(z^{-1})G(z^{-1})\|_\infty < 1$$

where $F_1(z^{-1})G(z^{-1}) \approx 1$ if the FIR filter inverse is accurate. Assuming $N > q$, the low-pass filter $H_1(z^{-1})$ can be chosen to be a linear-phase FIR filter with a delay of $N - q$, i.e., it will have an order of $2(N - q)$, which means that it will have $2(N - q) + 1$ taps.

3.2.2 Frequency Sampling FIR Filter Synthesis. The IPRF $H_3(z)$ as an FIR filter can also be found by taking the IDFT of $\hat{G}^{-1}(k)$. This method is also known as the frequency sampling method for FIR filter design [26]. The unit impulse response $g_i(n)$ of the inverse of the ETFE $\hat{G}^{-1}(k)$ is

$$g_i(n) = \frac{1}{M} \sum_{k=0}^{M-1} \hat{G}^{-1}(k) e^{j\frac{2\pi kn}{M}}$$

where $n \in [0, M - 1] \cap \mathbb{N}_0$. The IDFT is found in MATLAB using the function `ifft`. The FIR filter is then expressed in the z -domain as

$$\begin{aligned} F_2(z^{-1}) &= g_i(0) + g_i(1)z^{-1} + \dots + g_i(M-1)z^{-M+1} \\ &= \sum_{n=0}^{M-1} g_i(n)z^{-n} \end{aligned}$$

The frequency sampling method results in a unit impulse response which has been convoluted with a rectangular window of the same length in the frequency domain. The frequency response of $F_2(z^{-1})$ is therefore affected by the large side lobes of the rectangular window. As a result, the modeling error of $F_2(z^{-1})$ is large between the frequency samples. This can be alleviated by the use of a window that do not contain abrupt discontinuities in the time domain, and thus have small side lobes in the frequency domain, i.e., the window smooths the frequency response of $F_2(z^{-1})$.

A windowed FIR filter $\tilde{h}(n)$ is created from an unwrapped FIR filter $h(n)$ as

$$\tilde{h}(n) = w(n)h(n)$$

where $w(n)$ is a window function which is nonzero only for $n \in [0, M - 1] \cap \mathbb{N}_0$. The frequency domain representation of the window function $W(k)$ is found as

$$W(k) = \sum_{n=0}^{M-1} w(n - M/2) e^{-j\frac{2\pi kn}{M}} = \left[\sum_{n=0}^{M-1} w(n) e^{-j\frac{2\pi kn}{M}} \right] e^{-j\frac{2\pi kM}{2}}$$

where the term $e^{-j(2\pi k/M)(M/2)}$ comes from the fact that the rectangular window is not centered around $n=0$, but is time-shifted to be centered around $n=M/2$. This phase term will cause distortion of $h(n)$ unless $h(n)$ is also phase-shifted to compensate. The unit impulse response $g_i(n)$ is therefore phase-shifted before windowing. Due to the circular shift property of the DFT, this can be done by rearranging $g_i(n)$ such that

$$\tilde{g}_i(n) = \begin{cases} g_i(n + M/2), & n = 0, 1, \dots, \frac{M}{2} - 1 \\ g_i(n - M/2), & n = \frac{M}{2}, \frac{M}{2} + 1, \dots, M - 1 \end{cases}$$

for the case when M is even. The inverse response is then represented by the FIR filter

$$\bar{F}_2(z^{-1}) = \sum_{n=0}^{M-1} \tilde{g}_i(n) z^{-n} = z^{-M/2} F_2(z^{-1})$$

which is $F_2(z^{-1})$ delayed by $M/2$ steps. Applying the window $w(n)$ to the time-shifted impulse response $\tilde{g}_i(n)$

$$\tilde{g}_i(n) = w(n)\tilde{g}_i(n)$$

the filter

$$\tilde{F}_2(z^{-1}) = W(z^{-1}) * [z^{-M/2} F_2(z^{-1})]$$

is obtained, and $H_3(z^{-1}) = \tilde{F}_2(z^{-1})$ is used in Eq. (1).

For the implementation, $M=N$, and the stability criterion given in Eq. (6) is simplified by choosing

$$H_2(z^{-1}) = z^{-N/2} \quad (13)$$

since $|H_2(z^{-1})| = 1$, which results in

$$\begin{aligned} &\|z^{-N/2} - G(z^{-1})z^{-N/2}[F_2(z^{-1}) * W(z^{-1})]\|_\infty \\ &= \|1 - G(z^{-1})[W(z^{-1}) * F_2(z^{-1})]\|_\infty < 1 \end{aligned}$$

where $G(z^{-1})[W(z^{-1}) * F_2(z^{-1})] \approx 1$ if the FIR filter inverse is accurate. RC requires that the product of the filters $H_1(z^{-1})$ and $H_2(z^{-1})$ has a delay of N steps. Hence, $H_1(z^{-1})$ is chosen to be a linear-phase FIR filter with a delay of $N/2$ steps, i.e., it will have $N + 1$ taps. $H_1(z^{-1})$ is a low-pass filter used to satisfy Eq. (4) at higher frequencies, where the uncertainty of the FIR filter inverse is high, just as in the two previous cases.

4 System Identification

The quality of the resultant inverse response filters discussed above depends in large part on whether or not an accurate ETFE [21] of the plant can be obtained. The ETFE can be used to identify the coefficients in both IIR and FIR filters. For IIR filters, this is perhaps most commonly done using an output error model structure and an estimation method such as the least-squares method, or a subspace method [20,21]. The functions `tftest` or `n4sid` in MATLAB can be used to identify an IIR filter. Synthesizing an arbitrary FIR filter suitable for RC was discussed above: the filter coefficients can be found directly from the ETFT using a least-squares fit, or by direct frequency sampling with windowing.

Using ETFE for identification means that the model fit is done in the frequency domain. It is also possible to do identification in the time domain. The main advantage of using frequency domain data is that the FIR filter synthesis is simpler. Another advantage is that an almost arbitrary signal-to-noise ratio can be achieved by measuring single frequencies using the correlation method [21]. However, here two methods for generating the ETFE using wide-band excitation are presented, as collecting datasets for these methods is typically much less time-consuming and less error prone in practice.

4.1 Welch's Averaged Periodogram. In Refs. [19,22], and [23] the ETFE is obtained using Welch's averaged periodogram method [25]. The output data is usually then generated using Gaussian white noise excitation, although more informative input signals can be generated by experiment design, if prior information about the plant is known [21,29,30]. The ETFE of the plant $\hat{G}(k)$ and its inverse $\hat{G}^{-1}(k)$ are found as the quotient of the cross power spectral density estimate of the input and the measured output $P_{yu}(k)$, and the power spectral density estimate of the input $P_{uu}(k)$, i.e.,

$$\widehat{G}(k) = \frac{P_{yu}(k)}{P_{uu}(k)}, \text{ and } \widehat{G}^{-1}(k) = \frac{P_{uu}(k)}{P_{yu}(k)}$$

In Welch's method, the time series data is divided into windowed segments, with an option to use overlapping segments, then a modified periodogram of each segment is computed, and the results are then averaged [25]. Welch's method for generating an ETFE corresponds to the function `tffestimate` in `MATLAB`. The specific choice of windowing function, section overlapping, and number of frequency lines used, directly affects the quality of the estimate. The application of Welch's method can therefore tend to be tedious and computationally demanding. The variance in the estimate is approximately the inverse of the number of segments used. Welch's method can be applied recursively, computing and averaging the modified periodogram segmentwise. This reduces the memory requirements, but it must be done online while measuring the plant response.

4.2 Periodic Time-Domain Averaging. An alternative method for producing the ETFE is to use PRBS excitation and subsequent periodic averaging in the time domain. A PRBS is deterministic, periodic, and spectrally white. Moreover, a PRBS has an optimal crest factor which results in a large total energy delivery into the excited system. The periodicity makes it possible to average over several periods.

If the system is excited by a periodic repetition of the PRBS with length N for P periods, the total length of the output signal is NP . By averaging over the periods, the output signal has length N , but the signal-to-noise ratio is increased by a factor P [21]. This is approximately the same reduction in variance as can be obtained using Welch's method, however, less computation effort is required. The averaging is done online while measuring the plant response, but the computational effort is greatly reduced compared to a recursive implementation of Welch's method, as it is not required to compute the fast Fourier transform of each segment.

The ETFE of the plant and its inverse are then given as

$$\widehat{G}(k) = \frac{Y(k)}{U(k)}, \text{ and } \widehat{G}^{-1}(k) = \frac{U(k)}{Y(k)}$$

where $Y(k)$ and $U(k)$ are the DFT of, respectively, the output and input, i.e.,

$$Y(k) = \sum_{n=0}^{M-1} y(n)e^{-j2\pi kn/M} \text{ and } U(k) = \sum_{n=0}^{M-1} u(n)e^{-j2\pi kn/M}$$

for $k \in [0, M-1] \cap \mathbb{N}_0$. The DFT can be found in `MATLAB` using the `fft` function.

Since the data set is generated by recursive averaging, the memory requirements are modest, and since only the resultant average time series of length N is needed to produce the DFT, it is not computationally demanding. An almost arbitrary signal-to-noise ratio can be achieved by letting the averaging run for a long time. Since there are no variables in the method, the results will be consistent.

5 Estimating Tracking Performance

The RC tracking performance can be estimated by computing the average power of the error signal $e(n)$ when using a given periodic reference $r(n)$ and sensitivity function $S(z^{-1})$. Any real L -periodic discrete-time signal $x(n)$ can be represented by a Fourier series with L harmonic frequency components [31]

$$x(n) = \sum_{k=0}^{L-1} c_k^x e^{j\frac{2\pi kn}{L}}$$

where c_k^x are the Fourier coefficients. For the signal $x(n)$, computing the average power P_x in the time domain and in the frequency domain is equivalent. This is called Parseval's theorem [31]

$$P_x = \frac{1}{L} \sum_{n=0}^{L-1} |x(n)|^2 \equiv \sum_{k=0}^{L-1} |c_k^x|^2 \quad (14)$$

Given the Fourier coefficients c_k^r for the reference signal $r(n)$ and the sensitivity function $S(z^{-1})$, the Fourier coefficients c_k^e for the error signal $e(n)$ are found as

$$c_k^e \equiv c_k^r S(e^{-j\frac{2\pi k}{L}}), k = 0, 1, \dots, L-1$$

and an estimate of the average power of $e(n)$ when the system is stationary can be evaluated using Eq. (14).

6 System Description

The experiments were conducted on the two-axis serial-kinematic nanopositioning stage shown in Fig. 4. Each axis contains a 12-mm long piezoelectric stack actuator (Noliac NAC2003-H12) with a free displacement of $12 \mu\text{m}$ at 200 V. The flexure design includes a mechanical amplifier to provide a total range of $30 \mu\text{m}$. The flexures also mitigate cross-coupling such that each axis can be controlled independently. More details on the design of this stage can be found in Ref. [32]. The displacement of the moving platform is measured by a Microsense 6810 capacitive gauge and 6504-01 probe, which has a sensitivity of $2.5 \mu\text{m}/\text{V}$. The stage is driven by a PiezoDrive PDL200 voltage amplifier with a gain of 20 V/V. The control law was implemented on a dSPACE DS1104 hardware-in-the-loop system via `SIMULINK` coder. The anti-aliasing and reconstruction filters were implemented using two Stanford Research System SR570 pre-amplifiers. The experiments were conducted using the x -axis. The sampling frequency of the system was 10 kHz and the reference was a 40-Hz triangle wave signal with range $\pm 5 \mu\text{m}$. Since $T_s = 0.0001 \text{ s}$ and $L = 0.025 \text{ s}$, the required delay (2) is $N = 250$.

7 Control Design

7.1 RC With ZPETC Inverse. An ETFE of the plant, $\widehat{G}(k)$, was obtained using the periodic time-domain averaging described in Sec. 4.2. Figure 5 shows the ETFE. For the purpose of control design, an IIR model was found using the subspace identification method provided by the function `n4sid` in `MATLAB` [21]. A range of model orders were evaluated, and the \mathcal{H}_2 -norm of the model error

$$\|\widehat{G}(k) - \widehat{G}_{\text{IIR}}(e^{-j\frac{2\pi k}{M}})\|_2$$

for each model is plotted in Fig. 6. The fit between the model and the ETFE improves as the model order increases. However, the

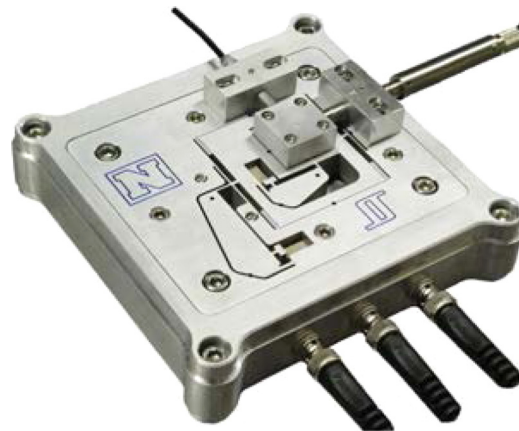


Fig. 4 Three-axis serial-kinematic nanopositioning platform [32]

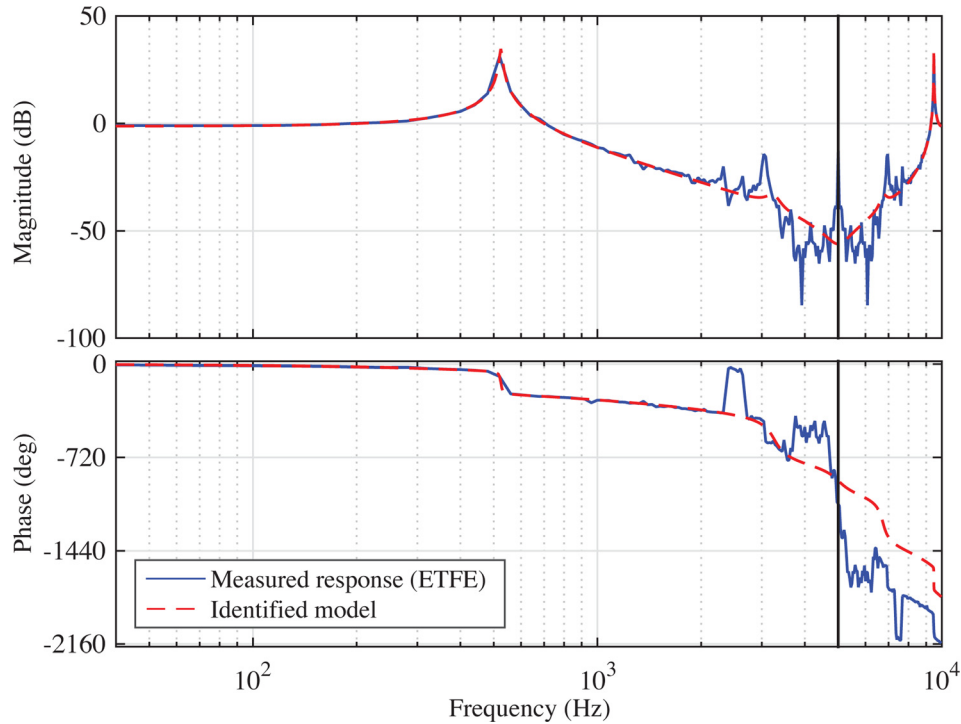


Fig. 5 The ETFE for the nanopositioner along the x -axis (solid line) and the frequency response of a fifth order IIR model found using subspace identification (dashed line)

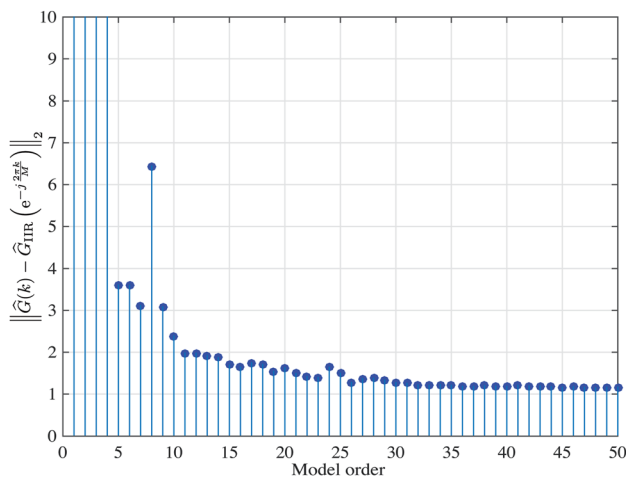


Fig. 6 The \mathcal{H}_2 -norm of the error between the ETFE and identified IIR models for model orders ranging from 1 to 50

magnitude response of the ZPETC inverse can become inaccurate since the ZPETC inverse excludes the nonminimum phase zeros. In Fig. 7, the number of nonminimum phase zeros for the identified models is plotted along with the \mathcal{H}_2 -norm error between the ETFE and the inverse of the ZPETC inverse. The number of nonminimum phase zeros tends to increase with the model order. From Fig. 7, the ZPETC inverse using a fifth-, sixth-, or seventh-order model provides a good fit, but lower and higher order models generate large model errors. For higher-order models, the nonminimum zeros tend to appear at high frequencies, and will therefore in this case not significantly impact the stability and performance since bandwidth-limited RC is used.

The cutoff frequency for $H_1(z^{-1})$ was chosen to be 1 kHz. This cutoff frequency would attenuate nonmodeled high-frequency dynamics and ensure that most of the models would provide a stability margin of at least 3 dB, i.e., the \mathcal{H}_∞ -norm in Eq. (4)

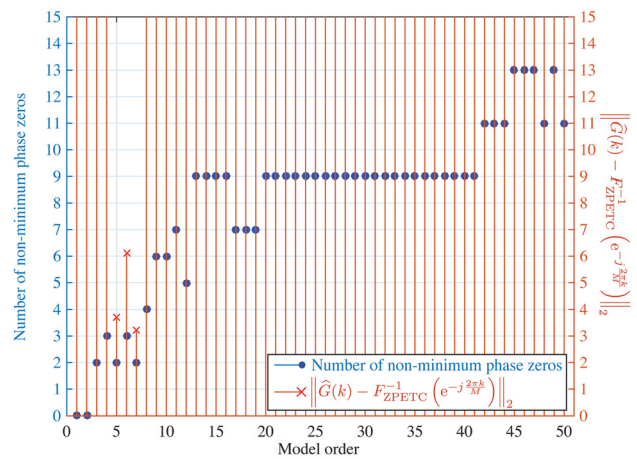


Fig. 7 The number of nonminimum phase zeros (left y-axis) and the \mathcal{H}_2 -norm error of the ETFE and inverse of the ZPETC model response (right y-axis) for model order ranging from 1 to 50

would be less than 0.7. This margin was chosen to accommodate for the hysteresis effect in the piezoelectric stack actuator. The hysteresis makes the gain dependent on the driving voltage, and this gain variation is not captured by the ETFE. The relationship between the model order and the stability criterion (4) is shown in Fig. 8.

If the system is stable, the tracking performance can be estimated by computing the average power of the error signal $e(n)$ using Eq. (14), as discussed in Sec. 5. The results when doing this for the ZPETC inverse are also shown in Fig. 8. It can be seen that the tracking performance does not improve significantly for model orders higher than five. This is because the RC performance is mostly determined by the zeros of the sensitivity function (3), which are limited by the cutoff frequency of the filter $H_1(z^{-1})$.

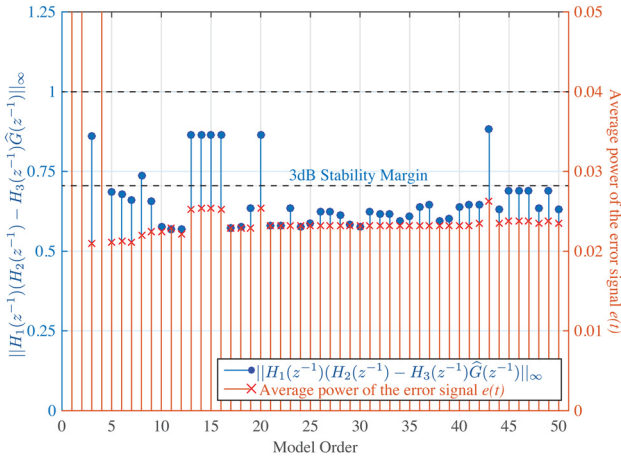


Fig. 8 The stability criterion plot of Eq. (4) for ZPETC inverse and low-pass filter $H_1(z^{-1})$ at cutoff frequency of 1 kHz for model orders ranging from 1 to 50 (left y-axis). The tracking performance for a 40 Hz triangular wave reference signal for model orders ranging from 1 to 50 (right y-axis).

The fifth-order model

$$\hat{G}_{\text{IIR}}(z^{-1}) = \frac{0.005z^{-1} + 0.01z^{-2} + 0.04z^{-3} + 0.05z^{-4} + 0.04z^{-5}}{1 - 1.52z^{-1} + 0.74z^{-2} - 0.85z^{-3} + 1.16z^{-4} - 0.38z^{-5}}$$

was chosen, as it was the lowest-order model with a 3 dB stability margin and had one of the lowest error power estimates. The frequency response of this model is shown in Fig. 5.

Figure 9 shows the frequency response of the ZPETC inverse together with the frequency response of the ETFE. It can be seen that the product of the ETFE and the ZPETC inverse is unity up to approximately 1 kHz.

The dead time of the system model is $d = 0$, and the numerator has $m_s = 1$ nonminimum phase zeros. The filters $H_3(z)$ and $H_2(z)$ are thus $H_3(z^{-1}) = z^{-1}F_{\text{ZPETC}}(z^{-1})$ and $H_2(z^{-1}) = z^{-1}$. As a result, the filter $H_1(z^{-1})$ has to have a delay of $N - (m_s + d) = 249$. The filter $H_1(z^{-1})$ is designed to be a linear-phase low-pass filter with a cutoff frequency of 1 kHz. The length of the filter is $2(N - (d + m_s)) + 1 = 499$, which results in the desired delay. Figure 10 shows the response of $H_1(z^{-1})$ and the stability criterion (4).

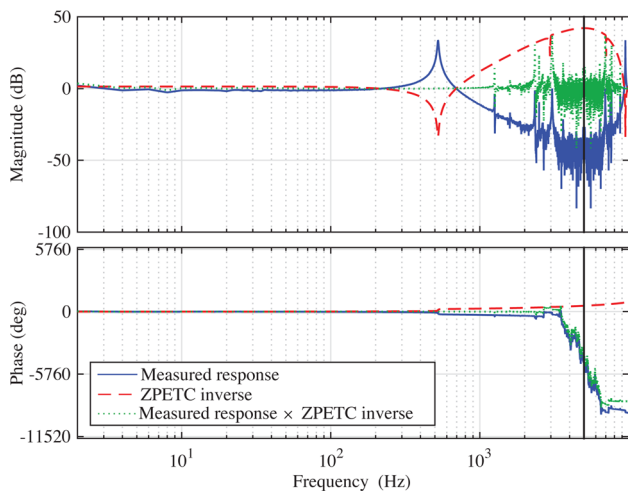


Fig. 9 Frequency responses for the ETFE, the ZPETC inverse, and the product of the two, when using a with a fifth-order model

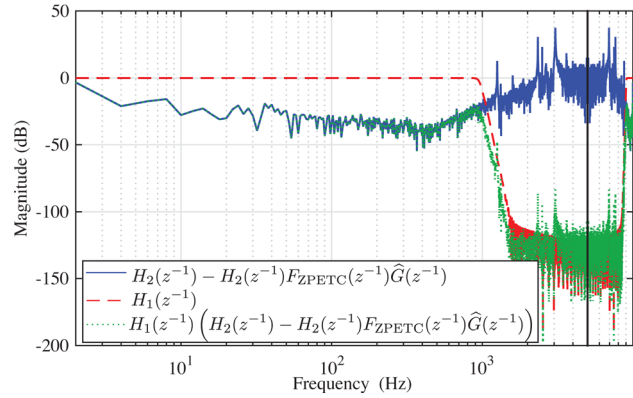


Fig. 10 The argument to the norms in the stability criteria (4), (5), and (6), when using a ZPETC inverse with a fifth-order model

7.2 RC With Optimization-Based FIR Filter.

Figure 11 shows frequency responses for the FIR inverse filter $H_3(z^{-1})$, found using the least-squares method, as described in Sec. 3.2.1. The ETFE was in this case obtained using Welch's method, discussed in Sec. 4.1, using the MATLAB function `tfestimate` with $M = 5000$ frequency samples from DC to the Nyquist frequency. The filter length was chosen to be $p = 30$, and hence $q = 15$. The reason for choosing this filter length is explained below.

Using an error weighting function set to unity $V(k) = 1$, the inverse filter provides a poor fit. As a result, the product of the ETFE and the FIR filter inverse is unity to approximately 100 Hz, which means that this is the usable RC bandwidth in this case. This is then almost equivalent of not having an inverse filter, i.e., $H_3(z^{-1}) = 1$.

To improve the obtained inverse response, the error weighting function $V(k)$ must be adjusted. Using $V(k) = 1$ in the optimization criterion (11) is not ideal, as there is an inherent error weighting emphasizing higher frequencies, since the amplitude of the frequency response of the inverse grows large as the frequency increases. For the measured frequency response displayed in Fig. 11, the error weighting function in Eq. (12) will provide better results, since it will counteract the increasing amplitude response of the inverse system. However, the results of using this weight are then dependent on the ETFE and can therefore give unexpected results depending on the quality and the specifics of the ETFE obtained. In this case, it is desirable to reduce the weight around the dominant resonance peak, in order to improve the fit

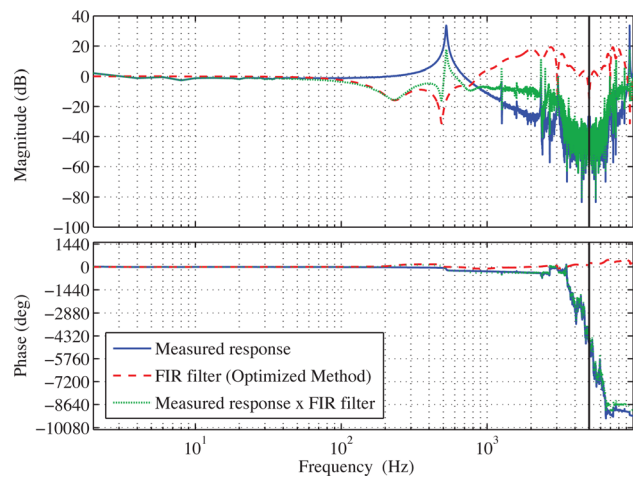


Fig. 11 Optimization-based FIR filter inverse frequency responses, with $p = 30$, $q = 15$, using the error weighting function $V(k) = 1$

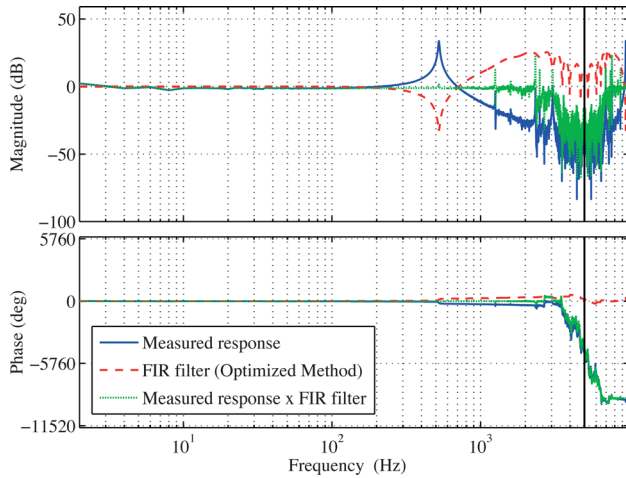


Fig. 12 Optimization-based FIR filter inverse frequency responses, with $p = 30$, $q = 15$, using the error weighting function (15)

elsewhere in the frequency domain. This should help to improve the match between the model and the plant and increase the stability margin. The error weighting function

$$V(k) = \begin{cases} 1 & \text{if } k \in [0, 500] \\ 0.1 & \text{if } k \in [501, 700] \\ 0.001 & \text{if } k \in [701, 1000] \\ 0.00001 & \text{if } k \in [1001, M - 1] \end{cases} \quad (15)$$

was used. This weighting was chosen based on trial and error not only to provide a good fit of the inverse response of the plant but also to ensure the system is stable. It takes into account that the uncertainty of the measurements increases as the frequency increases, since the gain of plant decreases at higher frequencies, decreasing the signal-to-noise ratio.

Figure 12 shows the frequency response of the optimization-based FIR filter inverse $H_3(z^{-1})$. The response of the filter provides a good fit. The product of the ETFE and the FIR filter inverse is unity to approximately 1 kHz, which is set as the cutoff frequency for the linear-phase low-pass filter $H_1(z^{-1})$ to attenuate the high-frequency dynamics which is poorly matched by the FIR filter.

Having chosen a weighting function $V(k)$, the stability and performance of this method rely on the choice of the filter length p . The relationship between the filter length and the stability criterion (4) is shown in Fig. 13. The cutoff frequency for $H_1(z^{-1})$ was fixed at 1 kHz, as it was difficult to obtain FIR filters that yielded a stability margin of 3 dB for higher cutoff frequencies. For the stable systems, the tracking performance was evaluated by the estimate of the average power of the error signal $e(n)$ using Eq. (14). This result is also plotted in Fig. 13. The tracking performance for different filter lengths is comparable as the performance is mostly determined by the cutoff frequency of the filter $H_1(z^{-1})$. The filter length of $p = 30$ was one of the shortest filters that provided a good stability margin.

In order to satisfy causality, the filters $H_3(z)$ and $H_2(z)$ are thus $H_3(z^{-1}) = z^{-15}F_1(z^{-1})$ and $H_2(z^{-1}) = z^{-15}$. As a result, the filter $H_1(z^{-1})$ has to have a delay of $N - q = 235$. The length of the filter is $2(N - q) + 1 = 470$, which results in the desired delay. Figure 14 shows the response of $H_1(z^{-1})$ and the stability criteria (4), (5), and (6). Compared with the filter shown in Fig. 11, the new filter provides a tenfold bandwidth increase.

7.3 RC With Frequency Sampling FIR Filter. Figure 15 shows the frequency response of the FIR inverse filter $H_3(z^{-1})$ found using the method described in Sec. 3.2.2. The ETFE of the

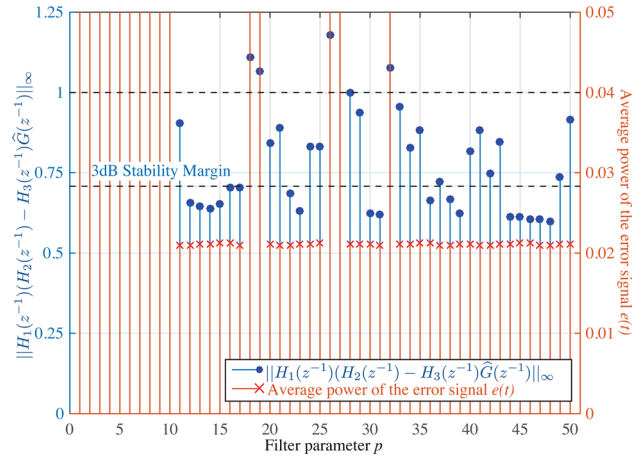


Fig. 13 The stability criterion plot of Eq. (4) for optimization-based FIR filter with error weighting (15) and low-pass filter $H_1(z^{-1})$ with cutoff frequency at 1 kHz for filter parameter p ranging from 1 to 50 (left y-axis). The tracking performance for a 40 Hz triangular wave reference signal (right) for the optimization-based FIR filter with error weighting (15) and filter parameter p ranging from 1 to 50 (right y-axis).

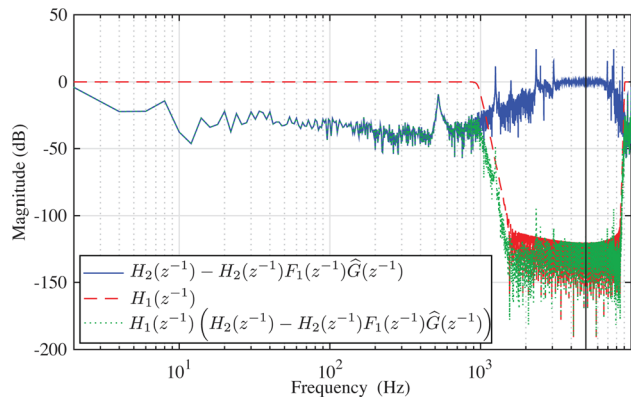


Fig. 14 The argument to the norms in the stability criteria (4), (5), and (6), when using an optimization-based FIR filter

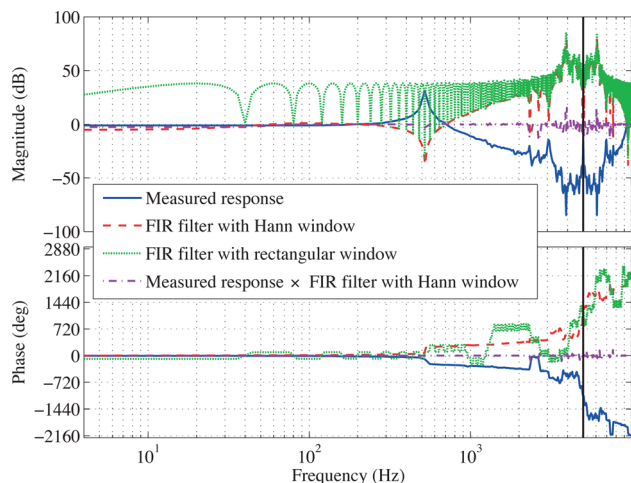


Fig. 15 Frequency sampling FIR filter inverse frequency responses, with rectangular and Hann windows

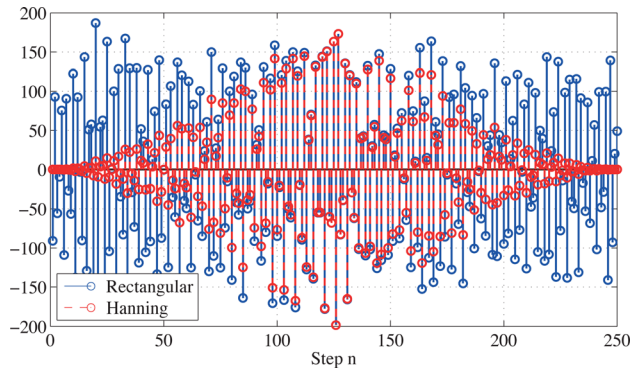


Fig. 16 The unit impulse response $h_3(n)$ when using a rectangular window and a Hann window

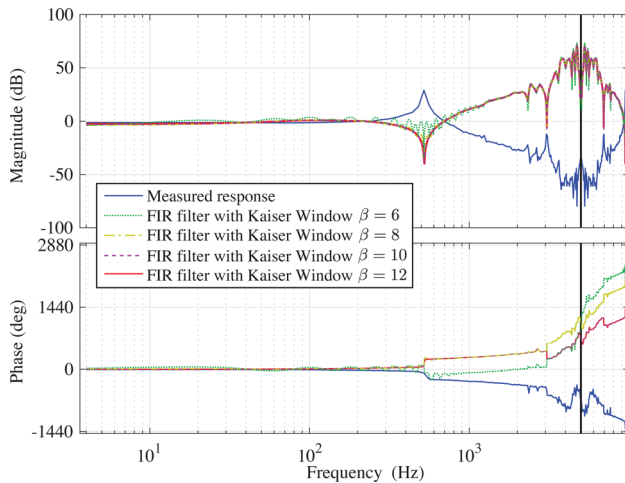


Fig. 17 Frequency sampling FIR filter inverse frequency responses, when using various Kaiser windows

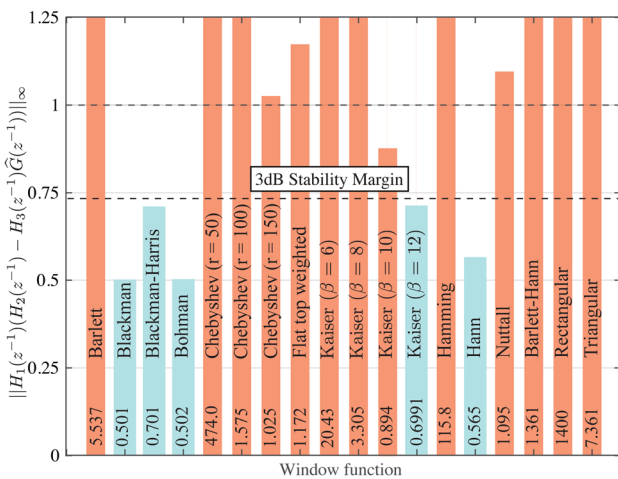


Fig. 18 The stability criterion plot of Eq. (4) for different window functions.

plant was again obtained using the periodic time-domain averaging in Sec. 4.2. For $H_3(z^{-1})$ with a rectangular window, the modeling error is zero at the frequency samples, $\{40, 80, 120, \dots\}$ Hz, but the error is large between the samples due to the large side lobes of the rectangular window. When applying a window, in this case a Hann window [33], to the FIR filter, the frequency

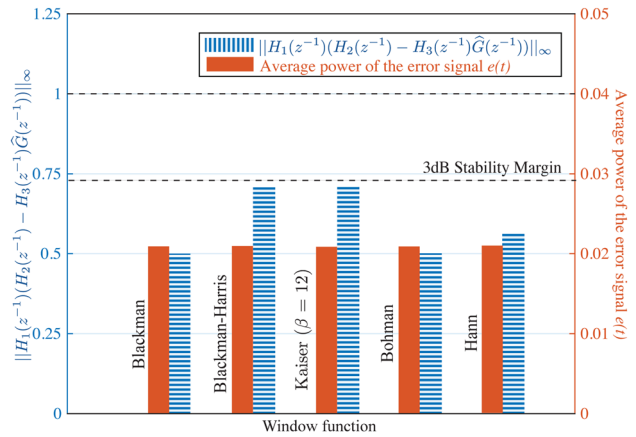


Fig. 19 The average power of the error signal for frequency sampling FIR filter with different window functions

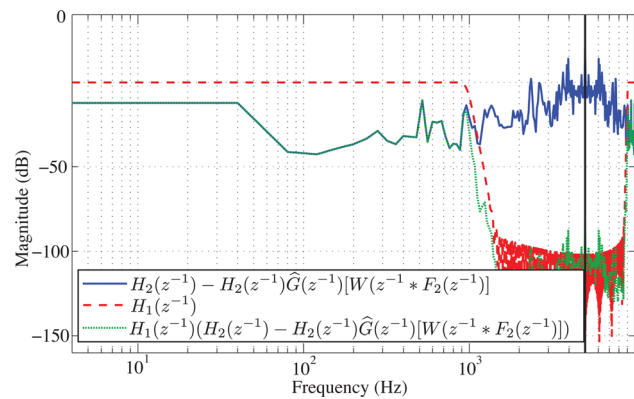


Fig. 20 The argument to the norms in the stability criteria (4), (5), and (6), when using a frequency sampling FIR filter (Hann window)

response is smoothed between the frequency samples. The product of the ETFE and $H_3(z^{-1})$ with a Hann window can be seen to be approximately unity up to about 1 kHz, similar to the case of the ZPETC inverse and the optimization-based FIR filter. The unit impulse responses, i.e., the FIR filter coefficients, when using rectangular and Hann windows are shown in Fig. 16.

To show the effect of the windowing, an adjustable window can be applied. A Kaiser window is given as [34]

$$w(n) = \frac{I_0\left(\beta\sqrt{1 - \left(\frac{n-N/2}{N/2}\right)^2}\right)}{I_0(\beta)}$$

where I_0 is the zeroth order modified Bessel function of the first kind and β is a non-negative real number that determines the shape of the filter. Figure 17 shows the inverse frequency response of the system when applying a Kaiser window with different values of β . The fit to the ETFE between the frequency samples is improved as β increases, since increasing β widens the main lobe width and decreases the amplitude of the side lobe.

In Fig. 18, the relationship between the stability criterion and different window functions, both fixed and adjustable, is shown. The cutoff frequency of filter $H_1(z^{-1})$ was set to 1 kHz, as it was difficult to obtain FIR filters that yielded a stability margin of 3 dB for higher cutoff frequencies. For this case, only four window functions render a stable system with sufficient margin. The tracking performance was evaluated by the estimate of the average

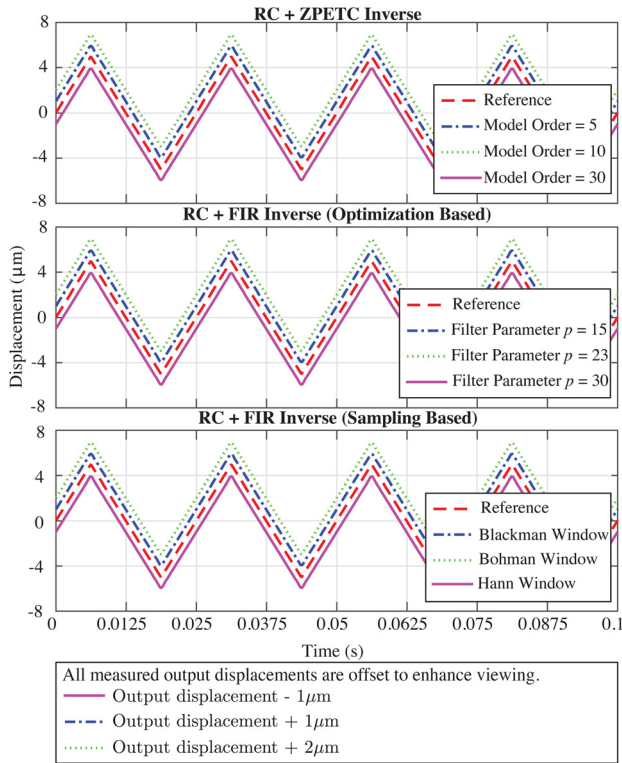


Fig. 21 The measured output displacements

power of the error signal $e(n)$ using Eq. (14). This result is plotted in Fig. 19. The tracking performance for different windows is comparable as the performance is mostly determined by the cutoff frequency of the filter $H_1(z^{-1})$.

The filter $H_2(z^{-1})$ has a delay of 125 steps, and the filter $H_1(z^{-1})$ is designed to be a linear-phase low-pass filter with delay of $N/2$ steps and a cutoff frequency of 1 kHz. The length of the filter is $N + 1 = 251$. Figure 20 shows the response of $H_1(z^{-1})$ and the stability criteria (4), (5), and (6).

8 Results

The reference signal is a $\pm 5 \mu\text{m}$ triangular wave at 40 Hz. The tracking performance of all three RC configurations is shown in Fig. 21, and the error plots are shown in Fig. 22. With $y(n)$ as the measured output and $r(n)$ as the reference and the error given as $e(n) = y(n) - r(n)$, the normalized maximum tracking error is defined as

$$e_{\max}(\%) = \frac{\max|e(n)|}{\max r(n) - \min r(n)} \times 100\%$$

The normalized root-mean-squared error (NRMSE) can be defined using Eq. (14) as

$$e_{\text{rms}}(\%) = \frac{\sqrt{P_e}}{\max r(n) - \min r(n)} \times 100\%$$

The relative error of the estimated tracking error is defined as

$$\text{Relative error}(\%) = \frac{|\text{Estimated } P_e - \text{Experimental } P_e|}{\text{Experimental } P_e} \times 100\%$$

The tracking performance results are summarized in Table 1.

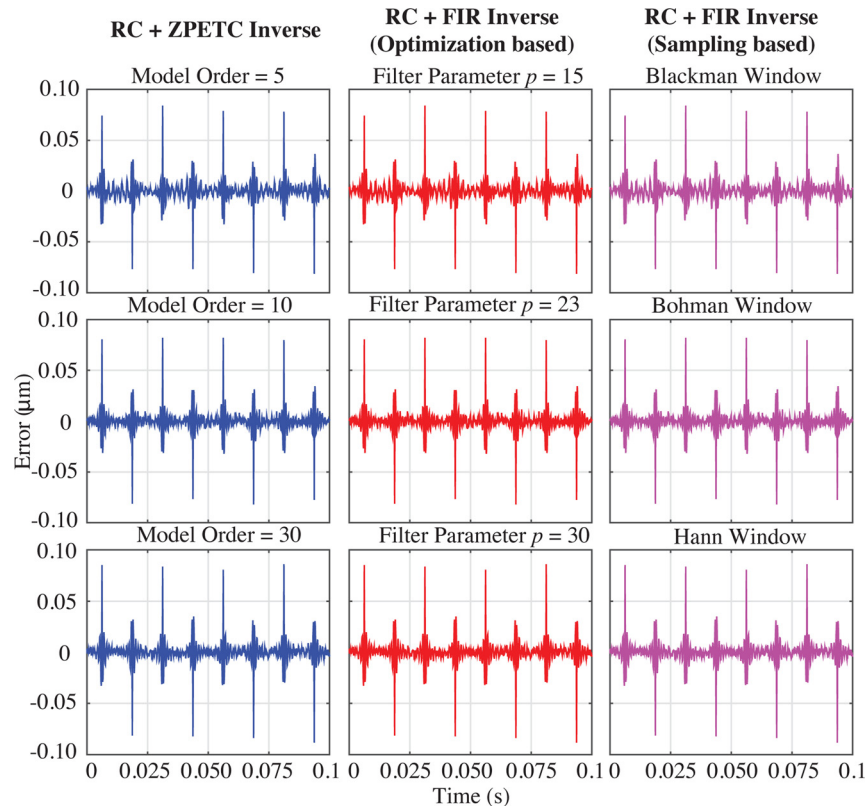


Fig. 22 The output displacement error

Table 1 Tracking performance for a $\pm 5 \mu\text{m}$ triangle wave at 40 Hz

Control law	Model order	e_{\max} (%)	e_{rms} (%)	Estimated P_e	Experimental P_e	Relative error (%)
RC with ZPETC inverse	5	0.888	0.105	0.0211	0.0284	27.0
	10	0.888	0.106	0.0224	0.0274	17.9
	30	0.941	0.110	0.0253	0.0300	15.9
Control law	Parameter p	e_{\max} (%)	e_{rms} (%)	Estimated P_e	Experimental P_e	Relative error (%)
RC with FIR inverse (optimization based)	15	0.888	0.103	0.0213	0.0269	20.8
	23	0.903	0.108	0.0211	0.0271	22.1
	30	0.896	0.105	0.0212	0.0267	20.6
Control law	Window	e_{\max} (%)	e_{rms} (%)	Estimated P_e	Experimental P_e	Relative error (%)
RC with FIR inverse (sampling based)	Blackman	0.873	0.102	0.0209	0.0269	22.3
	Bohman	0.888	0.102	0.0209	0.0263	20.5
	Hann	0.858	0.103	0.0209	0.0250	16.4

9 Discussion

In all three cases, the performances are comparable. However, the design process for the methods based on the ZPETC inverse and least-squares FIR filter synthesis can be cumbersome.

In order to design the filters needed in any of the RC implementations, an ETFE is needed. Two methods for obtaining an ETFE were presented: Welch’s method, and one using the DFT directly on time-domain data which has been periodically averaged. The latter method is recommended, as it will produce consistent results, as there are no variables in the application of the method. Furthermore, an almost arbitrary signal-to-noise ratio can be achieved with a very modest memory and computational cost. With effort, Welch’s method can be made to produce results matching the method using periodic time-domain averaging.

The first case of the inverse filters is model-based and requires an accurately identified model which not only depends on the choice of model structure but also on the excitation signal and the estimation method. In addition, nonminimum phase zeros, typically introduced due to sampling, cannot be inverted. Hence, the magnitude response of the ZPETC inverse can be inaccurate. As it turned out, a very good fit for a fifth-order model was found for the experimental system, and thus very good tracking results were obtained. However, this is not guaranteed in general. Higher order models were also considered. However, despite an improvement in the fit between the ETFE and identified IIR model, there was an increase in the number of nonminimum phase zeroes which resulted in a less accurate ZPETC inverse. Hence, the results in Table 1 show an increase in the normalized maximum and RMSE for higher-order models.

The alternative approach, using an FIR filter to model the inverse plant response, eliminates the issues of nonminimum

phase zeros and model structure selection. In the second case, an inverse response FIR filter was synthesized using frequency domain optimization. The tracking performance for filters with length $p \in \{15, 23, 30\}$ is compared in Table 1. The performances are comparable as the performance is mostly determined by the cutoff frequency of the filter $H(z^{-1})$. Better performances can ostensibly be obtained by choosing other filter lengths and adjusting the error weighting function in the least-squares optimization, as well as the adjusting the length of the time series, frequency lines, windowing function, and segment overlapping in Welch’s method.

In the third case, the results using Blackman, Bohman, and Hann windows are summarized in Table 1. The results are comparable as the performance is mostly determined by the cutoff frequency of the filter $H(z^{-1})$. However, the method proposed here provides a more direct route to synthesize a plant inverse FIR filter using the IDFT of the inverse of the ETFE of the plant. A suitable windowing function is applied to reduce artifacts due to the implicit rectangular windowing in the IDFT. Hence, the only variable in the method is the choice of windowing function. As was demonstrated, several windowing functions can be used to obtain a good inverse response filter, although some do not. The choice of windowing function is therefore crucial. With a suitable windowing function, the inverse filter yields similar or better tracking performance compared to the other two methods.

The computational complexity of each method is presented in Fig. 23 using the asymptotic notation. In addition, the computation time for the IPRF design in MATLAB is summarized in Table 2. The computation time of an ETFE using Welch’s average periodogram method is larger compared to the periodic time-domain averaging method. This is due to the size of the

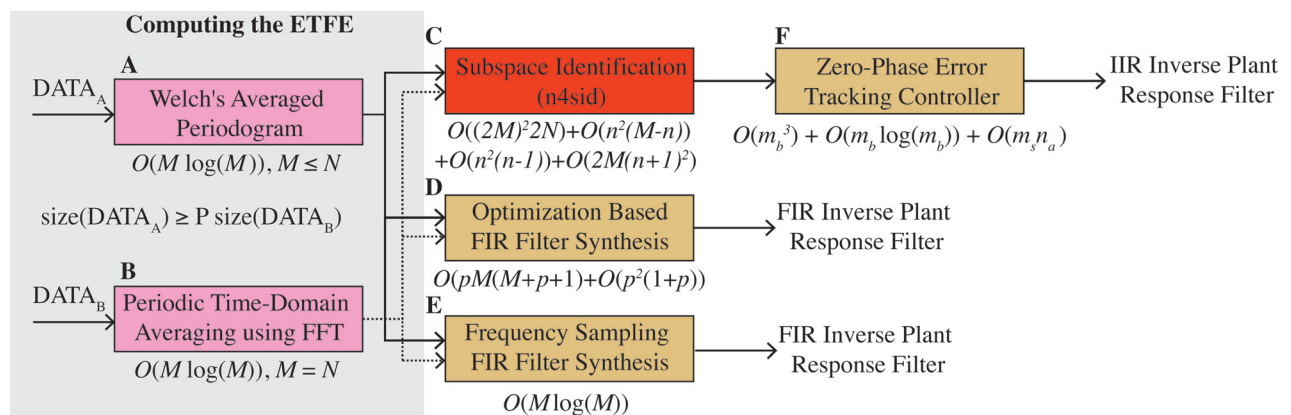


Fig. 23 Computational complexity of each method, using asymptotic notation

Table 2 Computation time of an IPRF design in MATLAB

Control law	Model order	Periodic time-domain averaging	System identification (n4sid)	ZPETC IIR filter
RC with ZPETC inverse	5	0.001 s	3.956 s	0.475 s
	10	0.001 s	3.901 s	0.485 s
	30	0.001 s	5.407 s	0.523 s
Control law	Parameter p	Welch's average periodogram	FIR filter (optimization)	
RC with FIR inverse (optimization based)	15	0.881 s	0.056 s	
	23	0.971 s	0.067 s	
	30	0.987 s	0.082 s	
Control law	Window	Periodic time-domain averaging	FIR filter (sampling)	
RC with FIR inverse (sampling based)	Blackman	0.001 s	0.003 s	
	Bohman	0.001 s	0.003 s	
	Hann	0.001 s	0.003 s	

data set required for Welch's method. For the ZPETC inverse, an IIR model is first required; hence, the subspace identification algorithm contributes to additional complexity and computation time. However, this step is not required for the FIR-based inverse filters. As for the computation time of the inverse filters, the complexity of the frequency sampling FIR filter is shown to be more efficient than the ZPETC inverse and optimization-based method as reported in Table 2.

10 Conclusion

This article focused on the design and implementation of a discrete-time RC scheme using a model-less FIR IPRF. Methods for obtaining an accurate ETFE and the synthesis of the FIR inverse from this estimate using the frequency sampling method were presented. The FIR inversion approach was compared to the more common approach of using an IIR filter inverse via the ZPETC method and an existing FIR design approach via frequency domain optimization. Experimental results showed that the proposed approach produced the same, or better, results than when using the ZPETC inverse or the optimization-based FIR filter inverse. However, the main advantage of using the proposed method is that it is a model-less approach, that is, no modeling effort is required, and it can alleviate problems due to nonminimum phase zeros. Furthermore, when compared to the existing FIR design approach, the proposed method only has one variable, the choice of windowing function, therefore simplifying the design process.

Acknowledgment

This project was supported by the Australian Research Council and the Norwegian University of Science and Technology.

References

- [1] Hara, S., Yamamoto, Y., Omata, T., and Nakano, M., 1988, "Repetitive Control System: A New Type Servo System for Periodic Exogenous Signals," *IEEE Trans. Autom. Control*, **33**(7), pp. 659–668.
- [2] Francis, B. A., and Wonham, W. M., 1976, "Internal Model Principle of Control-Theory," *Automatica*, **12**(5), pp. 457–465.
- [3] Inoue, T., Nakano, M., Kubo, T., Matsumoto, S., and Baba, H., 1981, "High Accuracy Control of a Proton Synchrotron Magnet Power Supply," 8th IFAC World Congress, Vol. 20, pp. 216–221.
- [4] Sato, H., Sueno, T., Toyama, T., Mikawa, M., Toda, T., and Matsumoto, S., 1991, "High Accuracy Magnet Power Supply for Proton Synchrotron by Repetitive Control," 22nd Annual IEEE Power Electronics Specialists Conference, Cambridge, MA, June 24–27, pp. 812–816.
- [5] Inoue, T., Nakano, M., and Iwai, S., 1981, "High Accuracy Control of Servomechanism for Repeated Contouring," 10th Annual Symposium on Incremental Motion Control Systems and Devices, pp. 285–292.

- [6] Yamada, M., Riadh, Z., and Funahashi, Y., 1999, "Design of Discrete-Time Repetitive Control System for Pole Placement and Application," *IEEE/ASME Trans. Mechatron.*, **4**(2), pp. 110–118.
- [7] Lee, R. C. H., and Smith, M. C., 1998, "Repetitive Control Experiments for a CD Player," *American Control Conference*, Philadelphia, PA, June 21–26, pp. 2682–2684.
- [8] Moon, J.-H., Lee, M.-N., and Chung, M. J., 1998, "Repetitive Control for the Track-Following Servo System of an Optical Disk Drive," *IEEE Trans. Control Syst. Technol.*, **6**(5), pp. 663–670.
- [9] Steinbuch, M., Weiland, S., and Singh, T., 2007, "Design of Noise and Period-Time Robust High-Order Repetitive Control, With Application to Optical Storage," *Automatica*, **43**(12), pp. 2086–2095.
- [10] Kim, D. H., and Tsao, T.-C., 2000, "Robust Performance Control of Electrohydraulic Actuators for Electronic Cam Motion Generation," *IEEE Trans. Control Syst. Technol.*, **8**(2), pp. 220–227.
- [11] Fleming, A. J., Kenton, B. J., and Leang, K. K., 2010, "Bridging the Gap Between Conventional and Video-Speed Scanning Probe Microscopes," *Ultramicroscopy*, **110**(9), pp. 1205–1214.
- [12] Shan, Y., and Leang, K. K., 2013, "Design and Control for High-Speed Nanopositioning: Serial-Kinematic Nanopositioners and Repetitive Control for Nanofabrication," *IEEE Control Syst. Mag.*, **33**(6), pp. 86–105.
- [13] Aridogan, U., Shan, Y., and Leang, K. K., 2009, "Design and Analysis of Discrete-Time Repetitive Control for Scanning Probe Microscopes," *ASME J. Dyn. Syst. Meas. Control*, **131**(6), p. 061103.
- [14] Tomizuka, M., Tsao, T.-C., and Chew, K.-K., 1989, "Analysis and Synthesis of Discrete-Time Repetitive Controllers," *ASME J. Dyn. Meas. Control*, **111**(3), pp. 353–358.
- [15] Inoue, T., 1990, "Practical Repetitive Control System Design," 29th IEEE Conference on Decision and Control, Honolulu, HI, Dec. 5–7, pp. 1673–1678.
- [16] Yamamoto, Y., 1993, "Learning Control and Related Problems in Infinite-Dimensional Systems," *Essays on Control: Perspectives in the Theory and Its Applications*, H. L. Trentelman, and J. C. Willems, eds., Birkhäuser, Boston, MA, pp. 191–222.
- [17] Peery, T. E., and Özbay, H., 1993, "On H_∞ Optimal Repetitive Controllers," 32nd IEEE Conference on Decision and Control, pp. 1146–1151.
- [18] Li, J., and Tsao, T.-C., 2001, "Robust Performance Repetitive Control Systems," *ASME J. Dyn. Syst. Meas. Control*, **123**(3), pp. 330–337.
- [19] Osburn, A. W., and Franchek, M. A., 2004, "Designing Robust Repetitive Controllers," *ASME J. Dyn. Syst. Meas. Control*, **126**(4), pp. 865–872.
- [20] McKelvey, T., Akcay, H., and Ljung, L., 1996, "Subspace-Based Multivariable System Identification From Frequency Response Data," *IEEE Trans. Autom. Control*, **41**(7), pp. 960–979.
- [21] Ljung, L., 1999, *System Identification: Theory for the User*, 2nd ed., Prentice Hall, Upper Saddle River, NJ.
- [22] Panomruttanarug, B., and Longman, R. W., 2007, "Designing Optimized FIR Repetitive Controllers From Noisy Frequency Response Data," *Adv. Astronaut. Sci.*, **127**, pp. 1723–1742.
- [23] Longman, R. W., 2010, "On the Theory and Design of Linear Repetitive Control Systems," *Eur. J. Control*, **16**(5), pp. 447–496.
- [24] Selesnick, I. W., Lang, M., and Burrus, C. S., 1996, "Constrained Least Square Design of FIR Filters Without Specified Transition Bands," *IEEE Trans. Signal Process.*, **44**(8), pp. 1879–1892.
- [25] Welch, P. D., 1967, "The Use of Fast Fourier Transform for the Estimation of Power Spectra: A Method Based on Time Averaging Over Short, Modified Periodograms," *IEEE Trans. Audio Electroacoust.*, **15**(2), pp. 70–73.
- [26] Rabiner, L. R., 1971, "Techniques for Designing Finite-Duration Impulse-Response Digital Filters," *IEEE Trans. Commun. Technol.*, **19**(2), pp. 188–195.
- [27] Tomizuka, M., 1987, "Zero Phase Error Tracking Algorithm for Digital Control," *ASME J. Dyn. Syst. Meas. Control*, **109**(1), pp. 65–68.
- [28] Gentle, J. E., 1998, *Numerical Linear Algebra for Applications in Statistics*, Springer-Verlag, New York.

- [29] Mareels, I. M. Y., Gevers, M., Bitmead, R. R., Lygeros, J., Kosut, R. L., and Poubelle, M. A., 1987, "How Exciting Can a Signal Really Be?," *Syst. Control Lett.*, **8**(3), pp. 197–204.
- [30] Rojas, C. R., Welsh, J. S., Goodwin, G. C., and Feuer, A., 2007, "Robust Optimal Experiment Design for System Identification," *Automatica*, **43**(6), pp. 993–1008.
- [31] Proakis, J. G., and Manolakis, D. G., 1995, *Digital Signal Processing*, Prentice Hall, Upper Saddle River, NJ.
- [32] Kenton, B. J., and Leang, K. K., 2012, "Design and Control of a Three-Axis Serial-Kinematic High-Bandwidth Nanopositioner," *IEEE/ASME Trans. Mechatron.*, **17**(2), pp. 356–369.
- [33] Harris, F. J., 1978, "On the Use of Windows for Harmonic Analysis With the Discrete Fourier Transform," *Proc. IEEE*, **66**(1), pp. 51–83.
- [34] Kaiser, J. F., 1974, "Nonrecursive Digital Filter Design Using the I_0 -sinh Window Function," IEEE International Symposium on Circuits & Systems, San Francisco, CA, Apr. 20–23, pp. 20–23.